Journal of Electroceramics 1:1, 27–39, 1997
© 1997 Kluwer Academic Publishers, Boston. Manufactured in The Netherlands.

Mn-doped $BaTiO_3$: Electrical Transport Properties in Equilibrium State*

JAE-YOUNG KIM,† CHANG-ROCK SONG & HAN-ILL YOO
School of Materials Science and Engineering, Seoul National University, Seoul 151–742, Korea

Received September 11, 1996; Revised December 19, 1996; Accepted January 7, 1997

Abstract. The electrical conductivity and thermoelectric power of Mn-doped $BaTiO_3$ (1 mole%) and ''undoped'' $BaTiO_3$ have been measured as functions of oxygen partial pressure (in the range of 10^{-16} to 1 atm) and temperatures (in the range of 900 to 1200°C), and compared with each other to differentiate the effect of the Mn-addition. It is found that the isothermal conductivity of Mn-doped $BaTiO_3$ varies with increasing Po_2 as $\sigma \propto Po_2^{-1/4}$ to $\propto Po_2^{-1/6}$ to $\propto Po_2^{+1/6}$, unlike previously reported. This behavior is well explained by the shift of the ionization equilibrium, $Mn_{Ti}^{x} = Mn_{Ti}' + h^{\cdot}$. The corresponding equilibrium constant, K_A, is determined from the Po_2 values demarcating those three different Po_2 regions as $K_A/cm^{-3} = 3.19 \times 10^{22} \exp(-1.69\,eV/kT)$. Basic parameters involving carrier density and mobility, and defect structure of Mn-doped $BaTiO_3$ are discussed in comparison with those of undoped $BaTiO_3$.

Keywords: Mn-doped $BaTiO_3$, electrical conductivity, thermopower, defect structure

I. Introduction

It has long been known that the addition of transition metal ions, e.g., Mn, Fe, and Cr, causes a pronounced enhancement of the positive-temperature-coefficient resistivity (PTCR) effect of $BaTiO_3$. Among them, Mn is the most effective: the enhancement of the electrical resistivity crossing the Curie point amounts to 4 to 5 orders of magnitude compared to undoped $BaTiO_3$ [1,2]. The effect of Mn-addition on properties of $BaTiO_3$ has thus been the subject of numerous studies [3–6], which are mostly concerned with the effect on PTCR and its enhancement mechanisms.

The defect chemical role of Mn, however, is not yet completely understood. Desu and Subbarao [7] have proposed that Mn (normally substituting *Ti* as tetravalent or Mn_{Ti}^{x}) may be reduced to a trivalent ion acting as an acceptor, Mn_{Ti}', when the surrounding oxygen partial pressure and/or temperature decreases. Hagemann and Hennings [8] have demonstrated via thermogravimetry the valence change of the Mn-dopant to acceptors with decreasing oxygen partial pressure in 1 *m/o* Mn-doped $BaTiO_3$. Recently, Osawa et al. [9] have first reported the equilibrium electrical conductivity of 2 *m/o* Mn-doped $BaTiO_3$ and interpreted its variation with oxygen partial pressure on the basis of the shift of the ionization equilibrium between tetravalent and trivalent Mn ions.

In order to better understand the defect-chemical role of Mn, we have closely examined the electrical transport properties including the electrical conductivity and thermopower for both Mn-doped $BaTiO_3$ and ''undoped''‡ $BaTiO_3$. In this paper, we will compare the equilibrium state properties of ''undoped'' $BaTiO_3$ and Mn-doped $BaTiO_3$. The purpose of this work is to understand the effect of Mn on defect structure of $BaTiO_3$ and its semiconducting properties in equilibrium.

*Based in part on the thesis submitted by J.-Y. Kim for the M.S. degree, Seoul National University, February, 1995.
†Now with Hyundai Electronics Industries Co., Ltd.
‡''undoped'' means not doped intentionally, but containing native impurities.

II. Experimental Procedures

Both ''undoped'' $BaTiO_3$ and Mn-doped $BaTiO_3$ (1 mole%) were prepared via a conventional powder processing route. Starting powders (all from Aldrich, U.S.A.), $BaTiO_3$ (99.9% pure), TiO_2 (99.99%) and MnO_2 (99.99%) were intimately mixed in the ratios, 1.000/0.001/0.000 (''undoped'' $BaTiO_3$) and 1.000/0.001/0.010 (Mn-doped $BaTiO_3$), respectively, by wet-milling in an ethanol media for 24 h and then by dry-milling with zirconia balls. The mixed powders were molded into discs, ca. 25 mm dia., under a uniaxial pressure of 10 MPa and then pressed cold-isostatically under 100 MPa for 2 min. Sintering was followed at 1350°C in air for 5 h. The as-sintered $BaTiO_3$ samples were found to be phase-pure by X-ray diffractometry. Their stoichiometric compositions may thus be represented as $Ba_{0.999}TiO_{2.999}$ and $Ba_{0.989}Ti_{0.990}Mn_{0.010}O_{2.989}$ for ''undoped'' $BaTiO_3$ and Mn-doped $BaTiO_3$, respectively. Both samples have the identical Ba/Ti ratio 0.999. One therefore expects that both samples have the same level of background impurities.

The as-sintered samples were cut with a low speed saw into parallelepipeds measuring ca $2\,mm \times 2\,mm \times 15\,mm$ for conductivity and thermopower measurements. Equilibrium conductivity and thermopower were measured against oxygen partial pressure at 900, 1000, 1100, and 1200°C using a conventional 4-probe dc technique and a steady state technique, respectively. Details of these techniques are described elsewhere [10]. The ambient oxygen partial pressure (Po_2) was controlled in a range of 10^{-16} to 1 atm with N_2/O_2 or CO/CO_2 mixtures and monitored with zirconia-based electrochemical cells.

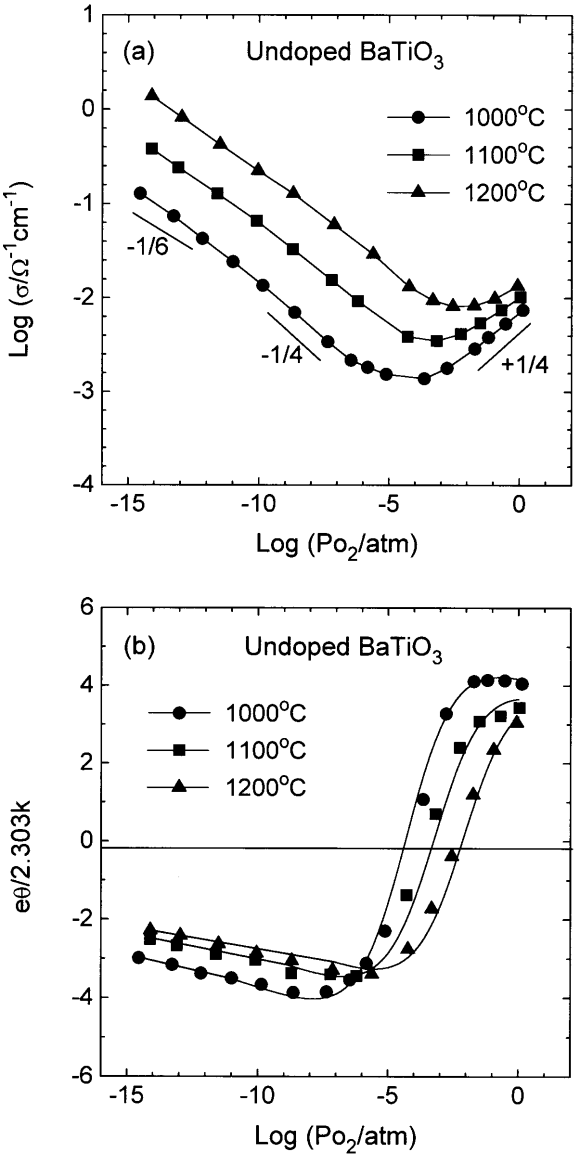

Fig. 1. Electrical conductivity (a) and thermopower (b) of ''undoped'' $BaTiO_3$ vs. oxygen partial pressure at different temperatures. The solid lines are for visual guidance.

III. Results

The results of the electrical conductivity (σ) and thermopower (θ) of ''undoped'' $BaTiO_3$ as a function of equilibrium Po_2 at different temperatures are shown in Figs. 1(a) and (b), respectively. From each of the conductivity isotherms, one may evaluate the oxygen-partial-pressure exponent of the conductivity, m_σ, which is defined as

$$m_\sigma = \left(\frac{\partial \log \sigma}{\partial \log Po_2}\right)_T \qquad (1)$$

It appears that m_σ changes from $-1/6$ to $-1/4$ (in the n-type regime) to $+1/4$ (in the p-type regime) as Po_2 increases in the range examined ($10^{-16} \leq Po_2/atm \leq 1$) at a given temperature. These data are in an excellent agreement with those reported in literature [11–16]. The thermopower changes its sign apparently at the identical Po_2 at which the corresponding conductivity assumes its minimum value, σ_m. Table 1 shows the values for the oxygen partial pressure (Po_2^o) corresponding to σ_m.

Table 1. Values of log (Po_2^o/atm) corresponding to σ_m for the two types of specimens

	log (Po_2^o/atm)	
T/°C	"undoped" $BaTiO_3$	Mn-doped $BaTiO_3$
900	—	−6.7
1000	−4.3	−5.3
1100	−3.2	−4.1
1200	−2.1	−3.1

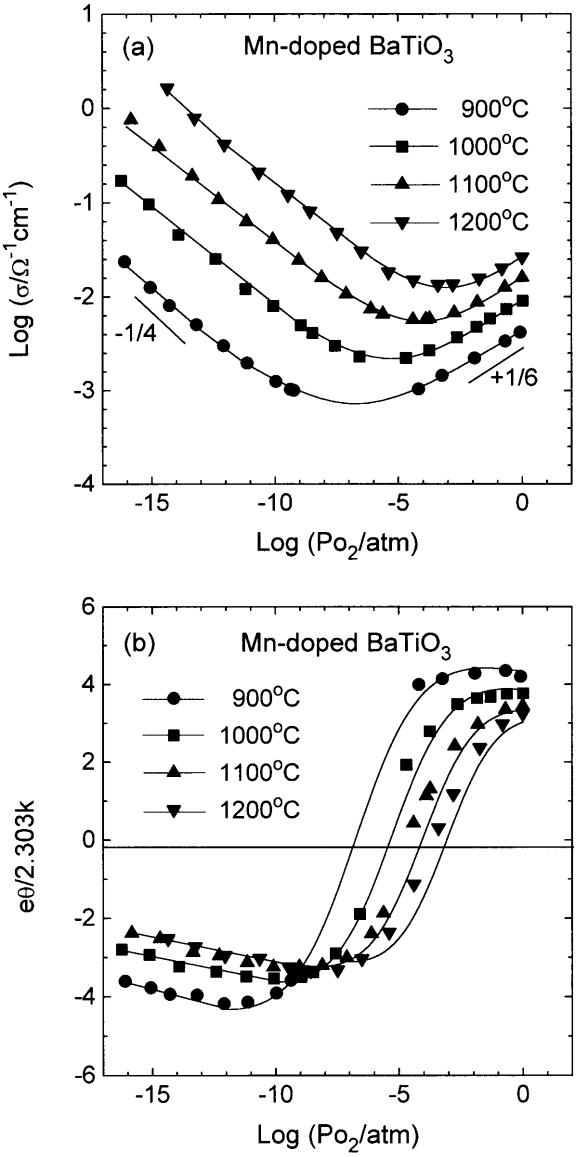

Fig. 2. Electrical conductivity (a) and thermopower (b) of Mn-doped $BaTiO_3$ vs. oxygen partial pressure at different temperatures. The solid lines are for visual guidance.

The results of the conductivity and thermopower for Mn-doped $BaTiO_3$ are shown in Figs. 2(a) and (b), respectively. Unlike the undoped specimens, the Po_2 exponent of the conductivity appears to be close to $m_\sigma = -1/4$ in the n-type regime and $m_\sigma = +1/6$ in the p-type regime, in general agreement with Osawa et al. [9]. The thermopower faithfully reflects a carrier type change from n-type to p-type crossing zero value at the oxygen partial pressures (Po_2^o) corresponding to σ_m (Table 1).

IV. Discussion

1. *Distinction of Mn-Effect*

Upon comparing the electrical conductivities of "undoped" $BaTiO_3$ (Fig. 1) and Mn-doped $BaTiO_3$ (Fig. 2), one can recognize that the positions of the conductivity minima (or $\theta = 0$) of Mn-doped $BaTiO_3$ have shifted systematically leftward compared to those for "undoped" $BaTiO_3$. The corresponding Po_2^o values are compared in Table 1.

Considering the only difference between these two types of specimens involves composition, the leftward shift of the conductivity minima is obviously attributed to the effect of the doped Mn on semiconducting properties of $BaTiO_3$. This effect is in agreement with literature reports [17–19] indicating that acceptors always result in a shift of the conductivity minimum to a lower Po_2 value. The behavior of Mn as an acceptor dopant in $BaTiO_3$ has long been recognized [20] and the present result reconfirms it.

The Mn-addition also appears to affect the Po_2-dependence of the equilibrium conductivity. As seen from the conductivity isotherms [Fig. 1(a)], m_σ assumes approximately $-1/6$, $-1/4$ and $+1/4$ in turn with increasing Po_2 for "undoped" $BaTiO_3$. Addition of Mn results in m_σ assuming approximately $-1/4$ and then $+1/6$ over the same oxygen partial pressure range [Fig. 2(a)].

A change in the Po_2-exponent of conductivity (m_σ) may be evaluated more precisely from the conductivity ratio $\alpha(=\sigma_p/\sigma_n)$ than from the total conductivity $\sigma(=\sigma_p+\sigma_n)$, σ_p and σ_n being the partial conductivity of holes (h) and electrons (e), respectively [21]. The conductivity ratio is calculated from the minimum conductivity, σ_m, and the total conductivity, σ, as [21,22]

$$\ln \alpha = 2 \cosh^{-1}\left(\frac{\sigma}{\sigma_m}\right) \tag{2}$$

Assuming the mobilities of electrons and holes are independent of carrier concentration, one may set

$$\sigma_n \propto n \propto \mathrm{Po}_2^{-|m_\sigma|}; \quad \sigma_p \propto p \propto \mathrm{Po}_2^{+|m_\sigma|} \tag{3}$$

due to the internal equilibrium,

$$0 = e' + h^{\bullet}; \quad K_i = np \tag{4}$$

where K_i is the corresponding equilibrium constant, and n and p are the concentration of electrons (e) and holes (h), respectively. Then,

$$\left(\frac{\partial \log \alpha}{\partial \log \mathrm{Po}_2}\right)_T = 2|m_\sigma| \tag{5}$$

Accordingly, this approach enables determination of the change in $|m_\sigma|$ with Po_2 with two times better resolution.

The plots of log α vs. log Po_2 for both ''undoped'' and Mn-doped $BaTiO_3$ are shown in Figs. 3(a) and (b), respectively. It is now clearly seen that each isotherm of α consists of two line segments with different slopes, $2|m_\sigma|$. Furthermore, the Mn-addition alters the log Po_2-dependence of log α of $BaTiO_3$ from elbow-downwardness to elbow-upwardness. This salient feature is emphasized in Fig. 4 notwithstanding the redundancy, where only the 1200°C isotherms for both types of specimens in Fig. 3 are coplotted for immediate contradistinction. As Po_2 increases at given temperatures, the slope $2|m_\sigma|$ changes from approximately 1/2 to 1/3 for Mn-doped $BaTiO_3$, whereas from $2|m_\sigma| = 1/3$ to 1/2 for ''undoped'' $BaTiO_3$.

The actual values for $2|m_\sigma|$ in both linear regions in Fig. 3 and the values for the oxygen partial pressure, Po_2^*, corresponding to the boundary between these two different slope regions are shown in Tables 2 and 3 for ''undoped'' and Mn-doped $BaTiO_3$, respectively. The latter Po_2^* values were calculated from the intersections of the two best-fitted lines. It is noted that the experimental slopes deviate very systematically from the ideal slopes, $2|m_\sigma| = 0.500$ and 0.333. It may result from the transition between the two limiting slopes, that is, the 0.500 slope makes the adjacent 0.333 slope look larger and the 0.333 slope makes the 0.500 slope look smaller.

It is noted that, for both types of specimens, the

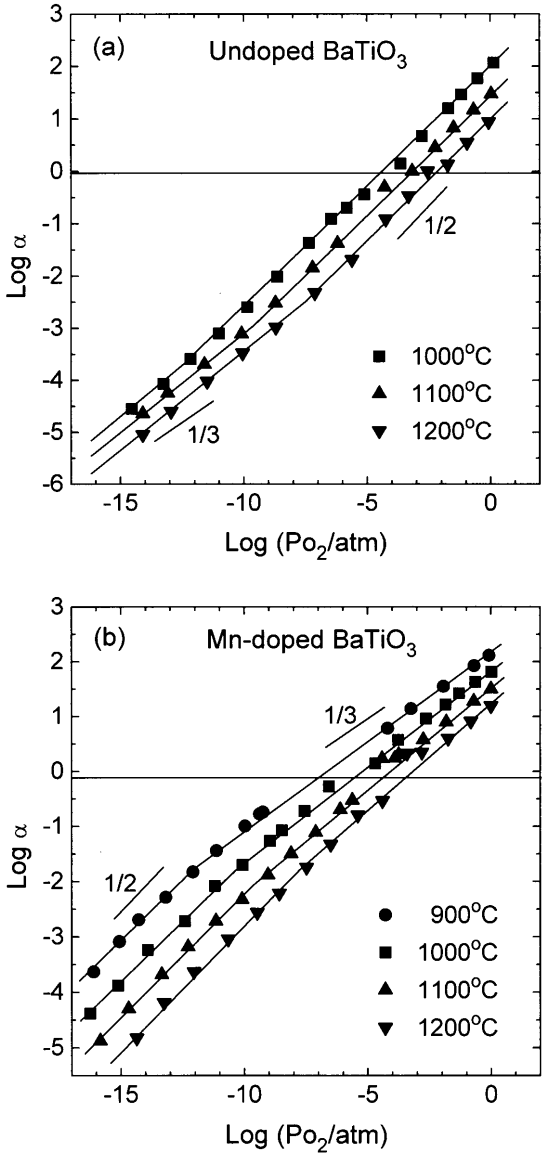

Fig. 3. Log α vs. oxygen partial pressure for ''undoped'' $BaTiO_3$ (a) and Mn-doped $BaTiO_3$ (b) at various temperatures. The solid lines are the best fitted.

oxygen partial pressure corresponding to the boundary between the two different slope ($2|m_\sigma|$) regions, Po_2^*, is always smaller by $4 \sim 5$ orders of magnitude than that corresponding to the conductivity minimum, Po_2°, at a given temperature, that is, $\mathrm{Po}_2^* < \mathrm{Po}_2^\circ$ (see Tables 1–3). This clearly indicates that there must be actually three Po_2 regions with different m_σ values on each of the isotherms in Figs. 1(a) and 2(a). They are:

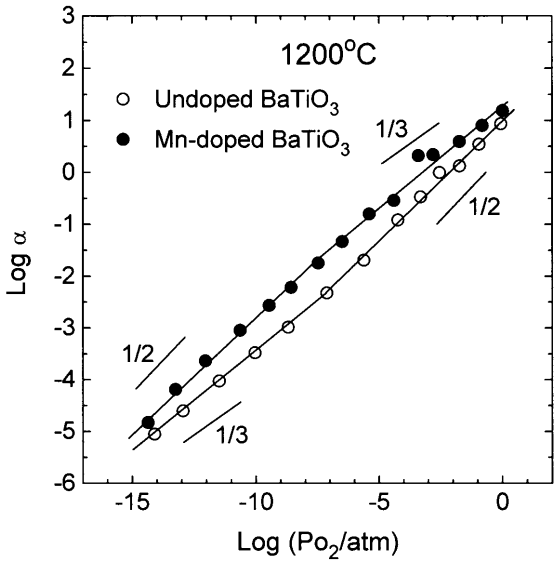

Fig. 4. Comparison of the 1200°C isotherms of α for ''undoped'' (○) and Mn-doped $BaTiO_3$ (●). Note the elbow-upward and elbow-downward characters of the Mn-doped and the ''undoped'', respectively.

Table 2. Values for the slope, $2|m_\sigma|$, in Fig. 3 and the boundary, Po_2^*, between the two different slope regions for ''undoped'' $BaTiO_3$

	$2\|m_\sigma\|$		
T/°C	$Po_2 < Po_2^*$	$Po_2 > Po_2^*$	$\log(Po_2^*/atm)$
1000	0.376§	0.469 ± 0.004	−12.06
1100	0.381 ± 0.003	0.470 ± 0.006	−9.43
1200	0.389 ± 0.002	0.472 ± 0.007	−7.18
ideal	0.333	0.500	

§ The uncertainty not evaluated due to limited number of data.

Table 3. Values for the slope, $2|m_\sigma|$, and the boundary, Po_2^*, between the two different slope regions for Mn-doped $BaTiO_3$

	$2\|m_\sigma\|$		
T/°C	$Po_2 < Po_2^*$	$Po_2 > Po_2^*$	$\log(Po_2^*/atm)$
900	0.46 ± 0.03	0.338 ± 0.003	−12.09
1000	0.45 ± 0.02	0.349 ± 0.004	−10.16
1100	0.461 ± 0.009	0.358 ± 0.006	−9.56
1200	0.46 ± 0.02	0.355 ± 0.010	−7.23
ideal	0.500	0.333	

for ''undoped'' $BaTiO_3$
(i) $m_\sigma = -1/6$ for $Po_2 < Po_2^*$,
(ii) $m_\sigma = -1/4$ for $Po_2^* < Po_2 < Po_2^\circ$,
(iii) $m_\sigma = +1/4$ for $Po_2^\circ < Po_2 \leq 1$ atm;
for Mn-doped $BaTiO_3$
(i) $m_\sigma = -1/4$ for $Po_2 < Po_2^*$,
(ii) $m_\sigma = -1/6$ for $Po_2^* < Po_2 < Po_2^\circ$,
(iii) $m_\sigma = +1/6$ for $Po_2^\circ < Po_2 \leq 1$ atm
It would be hard to discern the region (ii) directly from a total conductivity isotherm for Mn-doped $BaTiO_3$ in Fig. 2(a). In fact, Osawa et al. [9] report that the Po_2-exponent changes from $m_\sigma = -1/4$ (for $Po_2 < Po_2^\circ$) directly to $+1/6$ (for $Po_2 > Po_2^\circ$) with increasing Po_2 in the similar Po_2 range to the present. It is highly likely attributed to the poorer resolution associated with identifying the change in m_σ from a total conductivity isotherm rather than from the conductivity ratio isotherm.

2. *Basic Electronic Parameters*

Knowledge of the total conductivity (σ), the minimum conductivity (σ_m) and the thermopower (θ) measured simultaneously enables determination of the basic parameters of a semiconductor compound such as the concentrations of electronic carriers n and p, their mobilities μ_n and μ_p, and the band gap E_g. Below we will briefly consider terms describing semiconducting properties of Mn-doped $BaTiO_3$ for the sake of completeness.

(1) Band gap at 0 K, E_g^0. The minimum conductivity, that corresponds to $\alpha = 1$, may be written as [22]

$$\sigma_m^2 = 4K_i e^2 \mu_n \mu_p \tag{6}$$

where the equilibrium constant K_i defined in Eq. (4) is

$$K_i = N_c N_v \exp\left(-\frac{E_g}{kT}\right); \quad E_g = E_g^0 - \beta T \tag{7}$$

Here, N_c and N_v are the effective densities of states for electrons and holes, respectively, E_g^0 the band gap at the absolute temperature $T = 0$ K, and β the temperature coefficient of the band gap. Thus, disregarding the temperature dependence of the mobilities, we have

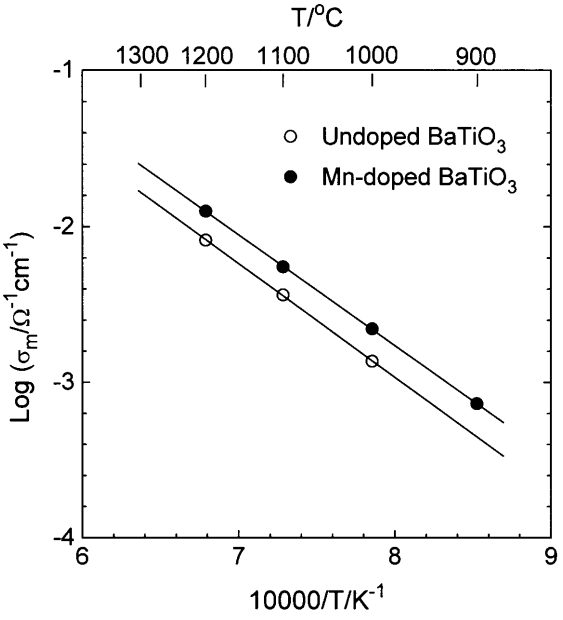

Fig. 5. The minimum conductivity vs. reciprocal temperature for ''undoped'' $BaTiO_3$ (○) and Mn-doped $BaTiO_3$ (●).

$$\frac{d\ln\sigma_m}{d(1/T)} = -\frac{E_g^0}{2k} \tag{8}$$

The minimum conductivity values for the Mn-doped $BaTiO_3$ and ''undoped'' $BaTiO_3$ are plotted against the reciprocal temperature in Fig. 5. The band gap at 0 K is found from the slopes as

$$E_g^0 = \begin{cases} 2.90 \pm 0.04 \text{ eV for ''undoped'' } BaTiO_3 \\ 2.82 \pm 0.01 \text{ eV for Mn-doped } BaTiO_3 \end{cases}$$

These values are compared with the band gaps reported in literature [11–13,15,16,23–28] in Table 4. They are in a reasonable agreement with those reported, but mark the smallest. One may argue that this would be due to the neglect of the ionic contribution to the minimum conductivity. But this possibility may be ruled out in the present case: The ionic contribution, σ_i, can be extracted, if any, by fitting the total conductivity, σ, in the Po_2-region around the minimum conductivity to the equation [29], $\sigma = \sigma_i + \sigma_n^0 Po_2^{-|m_\sigma|} + \sigma_p^0 Po_2^{+|m_\sigma|}$, where σ_n^0 and σ_p^0 are the *n*-type and *p*-type partial conductivities respectively at $Po_2 = 1$ atm. When the conductivity isotherms over the region $Po_2 > Po_2^*$ in Figs. 1(a) and 2(a) are thus best fit with $|m_\sigma| = 1/4$ and 1/6 for ''undoped'' and Mn-doped $BaTiO_3$, respectively, the excess conductivities (σ_i) turn out to be negative or otherwise $1 \sim 2$ orders of magnitude smaller than the minimum conductivity. In addition, they are subjected to a large uncertainty ($> \pm 50\%$) and do not exhibit any systematic dependence on temperature. This result clearly indicates that the present conductivities in Figs. 1(a) and 2(a) are essentially electronic. It is further substantiated by the fact that the total conductivity is completely commensurate with the corresponding thermopower, that is exclusively

Table 4. Comparison of the band gap energies reported on $BaTiO_3$

Author	E_g^0(eV)	Determined from	Measuring temperature (°C)	System	Ref.
Kim et al.	2.90 ± 0.04	σ_m vs. $1/T$	1000–1200	Polycrystal undoped $BaTiO_3$	this work
Kim et al.	2.82 ± 0.01	σ_m vs. $1/T$	900–1200	Polycrystal Mn-doped $BaTiO_3$	this work
Long and Blumenthal	3.10	σ_m vs. $1/T$	1000–1200	Polycrystal undoped $BaTiO_3$	11
Seuter	3.15	σ & θ Jonker's pear	600–1310	Polycrystal undoped $BaTiO_3$	12
Daniels and Härdtl	2.90	σ_m vs. $1/T$	1150–1250	Polycrystal undoped $BaTiO_3$	13
Eror and Smyth	3.27	σ_m vs. $1/T$	800–1200	Single crystal undoped $BaTiO_3$	15
Chan et al.	3.4	σ_m vs. $1/T$	750–1000	Polycrystal undoped $BaTiO_3$	16
Nowotny and Rekas	2.91 ± 0.13	σ & θ Jonker's pear	817–1037	Single crystal undoped $BaTiO_3$	23
Duverger et al.	2.96	σ_m vs. $1/T$	600–1000	Polycrystal undoped $BaTiO_3$	24
DiDomenico, Jr. and Wemple	3.30	Optical absorption	139	Single crystal undoped $BaTiO_3$	25
Cardona	3.20	Reflectance spectra	25	Single crystal undoped $BaTiO_3$	26
Baer	3.25	Interband Faraday rotation	130	Single crystal undoped $BaTiO_3$	27
Lewis and Catlow	3.05	Computer simulation	—	$BaTiO_3$	28

electronic by the nature of measurement, via Eq. (9) or Jonker's pear analysis [30].

As seen from Fig. 5, addition of Mn results in an increase of the minimum conductivity by a factor of approximately 1.6. The minimum conductivity can increase if there is an enhanced contribution of ionic conduction due to acceptors. But this possibility is now ruled out in the present case. It may thus be attributed to the difference in the temperature dependence of the band gap energy, β in Eq. (7), that is likely to be caused by Mn addition. The typical value for β is on the order of 10^{-4} eV/K [12,23]. On the basis of Eq. (6), a difference in β on the order of 1×10^{-4} eV/K $(=\beta_{doped}-\beta_{undoped})$ results in the minimum conductivity for Mn-doped $BaTiO_3$ being larger than that of ''undoped'' $BaTiO_3$ by the factor of 1.8.

The band gap, E_g^0, may also be estimated from the thermopower by fitting θ vs. $\ln\alpha$ to the equation [21,31] that is essentially identical to Jonker's ''pear'' formalism [30]:

$$\frac{2e\theta}{k}=\varepsilon\tanh\left(\frac{1}{2}\ln\alpha\right)-\ln\alpha+\delta \tag{9}$$

where the fitting parameters ε and δ are respectively defined as

$$\varepsilon=\frac{E_g^0}{kT}-\frac{\beta}{k}+A_n+A_p \tag{10}$$

$$\delta=\ln\frac{N_v\mu_p}{N_c\mu_n}+A_p-A_n \tag{11}$$

Here, A_n and A_p are the kinetic parameters (involving the entropies of transport) for electrons and holes, respectively [21,22,30]. The band gap E_g^0 can thus be evaluated from the slope of ε vs. $1/T$.

The results of fitting, $2e\theta/k$ vs. $\ln\alpha$, are shown in Figs. 6(a) and (b) for ''undoped'' and Mn-doped $BaTiO_3$, respectively. The parameters ε are plotted against $1/T$ in Fig. 7. As is the case with fitting to Eq. (9) [21], ε is subjected to a larger scatter than the minimum conductivity. The band gap, E_g^0, and the term, $-\beta/k+A_p+A_n$, evaluated in accord with Eq. (10) are listed in Table 5. The values of E_g^0 determined here are in a reasonable agreement with those determined from the conductivity minima, see Table 4. This agreement suggests that the carrier mobilities are temperature-insensitive in the temperature range examined. [See Eqs. (6) and (8).]

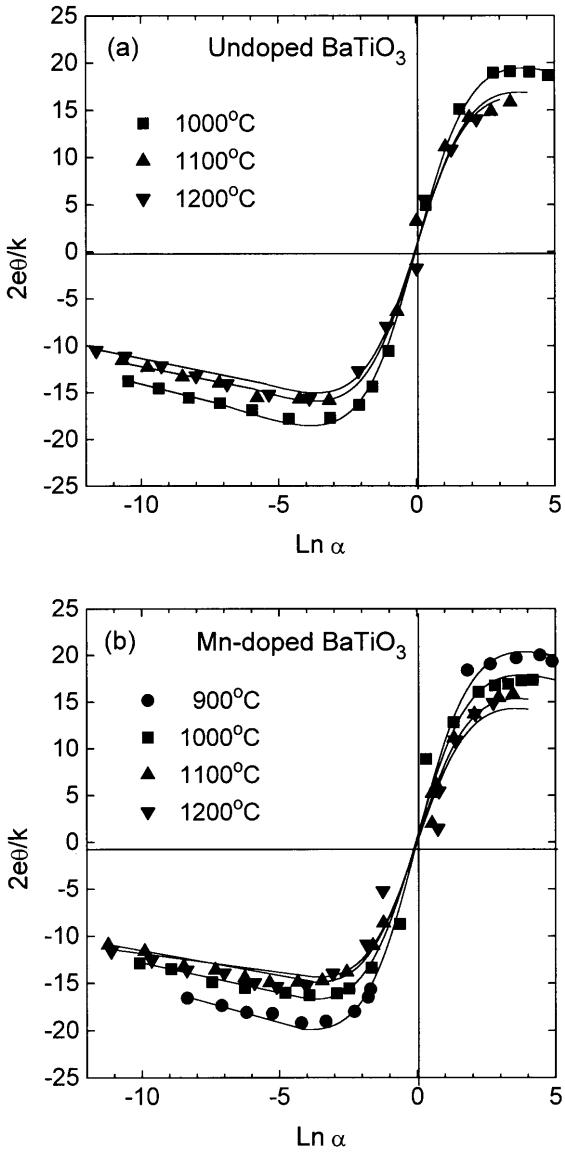

Fig. 6. Reduced thermopower, $2e\theta/k$, vs. $\ln\alpha$ for ''undoped'' $BaTiO_3$ (a) and Mn-doped $BaTiO_3$ (b). Solid lines are the best fitted to Eq. (9) in the text.

(2) Carrier mobilities. In principle, the carrier mobilities, μ_n and μ_p, can be evaluated from Eq. (11) and Eq. (6) combined with Eq. (7). However, one has to assume appropriate values for the densities of states, N_c and N_v, and the transport parameters, A_n and A_p, which depend on the conduction mechanism [22,30]. Furthermore, the parameter δ that is evaluated from Eq. (9) is often subject to a large uncertainty. The carrier mobilities therefrom are, therefore, not so

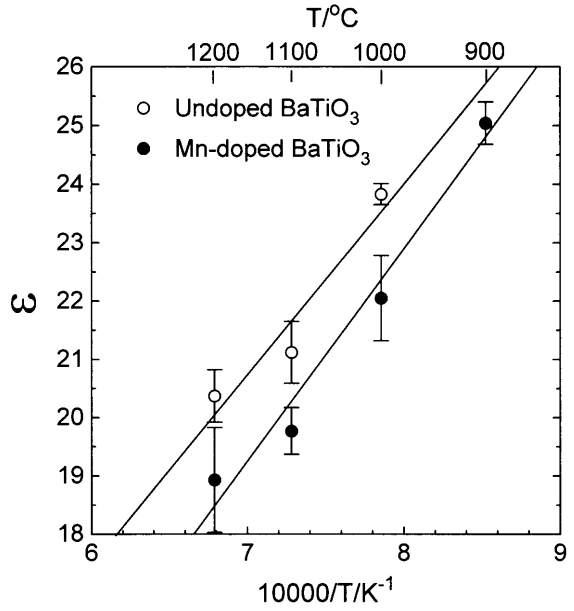

Fig. 7. Fitting parameter ε vs. reciprocal temperature for ''undoped'' $BaTiO_3$ (○) and Mn-doped $BaTiO_3$ (●).

Table 5. The forbidden gap, E_g^0, and the term, $-\beta/k + A_p + A_n$, for ''undoped'' $BaTiO_3$ and Mn-doped $BaTiO_3$

	''undoped'' $BaTiO_3$	Mn-doped $BaTiO_3$
E_g^0/eV	2.83 ± 0.80	3.11 ± 0.37
$-\beta/k + Ap + An$	-2.22 ± 0.70	-6.00 ± 0.55

highly reliable. Nevertheless, possible values for the mobility ratio $b(\equiv \mu_n/\mu_p)$ are documented below.

As seen from Fig. 6, δ is very close to zero at all temperatures. This simply indicates that the Po_2 values corresponding to δ_m and $\theta = 0$ nearly coincide as actually found in Figs. 1 and 2. Equation (11) thus leads to

$$b \approx \frac{N_v}{N_c} \exp(A_p - A_n) \tag{12}$$

Obviously, the mobility ratio b in Eq. (12) depends on the conduction mechanism. Nowotny [23] examined three possible mechanisms: (i) hopping conduction; (ii) band conduction; (iii) hopping conduction by electrons and band conduction by holes. Assuming the hopping conduction as the most plausible mechanism [12,32–35], we have: $A_p = A_n \approx 0$ [30]; $N_c = [Ti_{Ti}^x] \approx N_A V_m$ and $N_v = [O_O^x] \approx 3N_A/V_m$ (V_m being the molar volume of $BaTiO_3$ and N_A the Avogadro number) [23]. Thus, $b \approx 3$. In this case, Eq. (7) may be evaluated with the use of the representative value of E_g^0, 2.90 eV as

$$K_i/\mathrm{cm}^{-6} = N_c N_v \exp\left(\frac{-E_g}{kT}\right) = 6.8 \times 10^{44} \exp\left(-\frac{2.90\,\mathrm{eV}}{kT}\right) \tag{13}$$

Taking into account Eq. (6) and Eq. (13), we obtain: $\mu_n = 0.16\,\mathrm{cm}^2$/V-sec at the temperatures examined. In the literature are reported, e.g., $\mu_n = 0.2\,\mathrm{cm}^2$/V-sec at 1000 K [12], $0.14\,\mathrm{cm}^2$/V-sec at 1310 K [36] and $\mu_p = 0.02\,\mathrm{cm}^2$/V-sec at 700 K [12], $0.01\,\mathrm{cm}^2$/V-sec at 350 K [34], $0.02\,\mathrm{cm}^2$/V-sec at 1000°K [36].

3. *Defect Structure*

As seen from Figs. 1–3, the Po_2 exponent of the electrical conductivity, m_σ, assumes the values in sequence as Po_2 increases from 10^{-16} to 1 atm for ''undoped'' $BaTiO_3$:

$$\underset{\longleftarrow\ Po_2\ \longrightarrow}{-\frac{1}{6},\ -\frac{1}{4},\ +\frac{1}{4}} \tag{14}$$

For Mn-doped $BaTiO_3$, the corresponding sequence of m_σ is:

$$\underset{\longleftarrow\ Po_2\ \longrightarrow}{-\frac{1}{4},\ -\frac{1}{6},\ +\frac{1}{6}} \tag{15}$$

Each of these m_σ values is representative of a majority disorder type in the corresponding Po_2 region [37].

There have been proposed many defect models for $BaTiO_3$ [38]. We here assume that each sublattice of $BaTiO_3$ can accommodate vacancies such as V''_{Ba}, V''''_{Ti}, and $V_O^{\bullet\bullet}$ (in Kroeger-Vink notation). The possibility of interstitial defects may be precluded because they are energetically unfavourable in the perovskite structure [19,28,39]. We also assume that acceptor-type cation impurities A'_C should be taken into account. Therefore the following internal and external equilibria may be considered in addition to the internal excitation equilibrium, Eq. (4):

$$0 = V''_{Ba} + V''''_{Ti} + 3V_O^{\bullet\bullet} E$$
$$K_S = [V''_{Ba}][V''''_{Ti}][V_O^{\bullet\bullet}]^3 \tag{16}$$

$$0_o^x = V_O^{\bullet\bullet} + 2e' + \tfrac{1}{2}O_2(g);$$
$$K_R = [V_O^{\bullet\bullet}]n^2 Po_2^{1/2} \tag{17}$$

$$BaO = Ba_{Ba}^x + O_o^x + V_{Ti}^{''''} + 2V_O^{\bullet\bullet};$$
$$K_B = [V_{Ti}^{''''}][V_O^{\bullet\bullet}]^2 a_{BaO}^{-1} \tag{18}$$

where K_j $(j = S,R,B,)$ stands for the equilibrium constant of the corresponding reaction, a_{BaO} the activity of BaO, and $[k]$ the concentration of the irregular structure element k $(= V_{Ba}'', V_{Ti}'''', V_O^{\bullet\bullet}, A_C')$. It is noted that there should be two extrinsic equilibria, Eqs. (17) and (18) because the system is ternary [37]. We may write the following charge neutrality condition:

$$n + 2[V_{Ba}''] + 4[V_{Ti}''''] + [A_C'] = p + 2[V_O^{\bullet\bullet}] \tag{19}$$

Configuration of the majority disorder types depends on the thermodynamic variables of the system, Po_2 and a_{BaO}, at a given temperature. When the system is pure (i.e., $[A_C'] \ll [V_{Ba}''] + [V_{Ti}'''']$), then only two possibilities may be distinguished at the stoichiometric composition: (i) when electronic defects prevail ($K_S^{1/5} \ll K_i^{1/2}$); (ii) when ionic defects prevail ($K_S^{1/5} \gg K_i^{1/2}$). The overall configuration of the majority disorder types for the first case is reported in [40]. The second case is shown in Fig. 8(a). We believe that the second case is likely for pure $BaTiO_3$ since there are no experimental data supporting the presence of the majority electronic disorder (i.e., $n \simeq p$) for ''pure'' $BaTiO_3$ and since the oxygen exponents for ''pure'' $BaTiO_3$ [Eq. (14)] are in agreement with what Fig. 8(a) predicts (see below). When the system is doped intentionally or unintentionally with acceptors ($[A_C'] \gg K_S^{1/5}$ or $K_i^{1/2}$), only one configuration is allowed (irrespective of whether $K_S^{1/5} \ll K_i^{1/2}$ or $K_S^{1/5} \gg K_i^{1/2}$) and that is shown in Fig. 8(b). Concentrations of all the ionic and electronic defects can then be immediately calculated as functions of Po_2 and a_{BaO} in each majority defect regime at the given temperature by simultaneously solving Eqs. (4) and (16)–(19), but it is not completely pursued here. Only the Po_2-exponent, m_σ, of the major carrier density n or p will be considered below [see Eq. (3)].

One can immediately recognize that only either of the following two sequential configurations of majority disorder types with increasing Po_2 allows the sequence of m_σ values [Eq. (14)] for our ''undoped'' specimen $Ba_{0.999}TiO_3$:

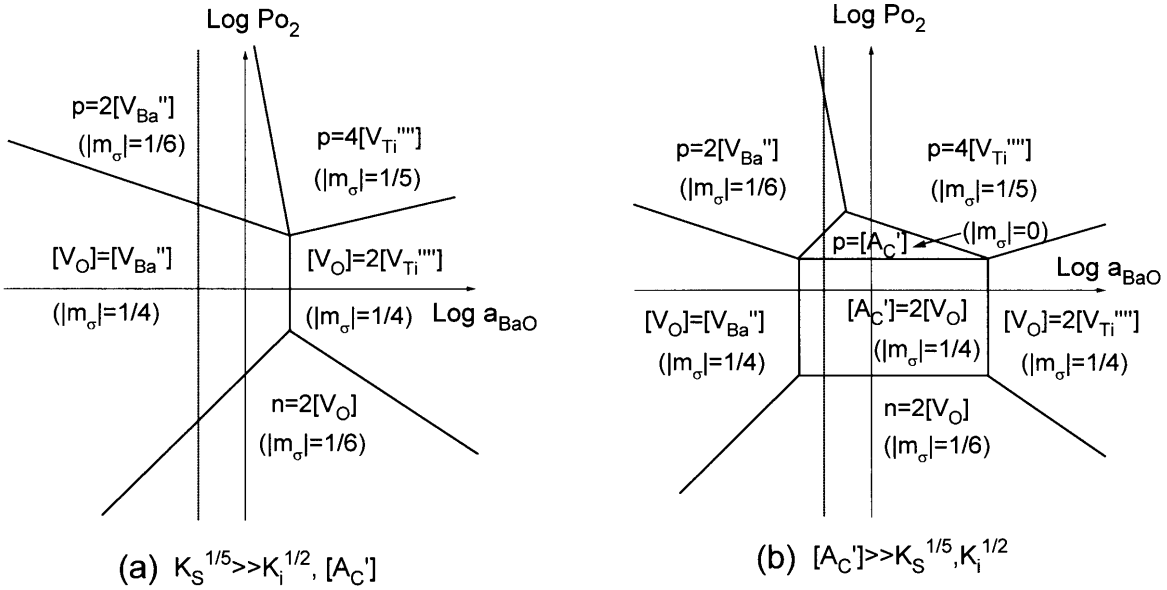

Fig. 8. Configuration of the majority disorder types depending on the thermodynamic variables log Po_2 and a_{BaO} at a given temperature: (a) when $K_S^{1/5} \gg K_i^{1/2}$, $[A_C']$; (b) when $[A_C'] \gg K_S^{1/5}$, $K_i^{1/2}$. $|m_\sigma|$ denotes the oxygen partial pressure exponent of electronic carrier densities such that $n \propto Po_2^{-|m_\sigma|}$ and $p \propto Po_2^{+|m_\sigma|}$. The dotted lines in (a) and (b) represent the possible paths allowing the sequences of $|m_\sigma|$ values in Eqs. (14) and (15), respectively, as observed experimentally.

(i) When the system is really pure (i.e., $[A'_C] \ll [V''_{Ba}]$)

majority disorder	$n = 2[V_O^{\bullet\bullet}]$	$[V_O^{\bullet\bullet}] = [V''_{Ba}]$	$p = 2[V''_{Ba}]$
m_σ	$-1/6$	$-1/4, \quad +1/4$	$+1/6$
	———	Po_2 ———	⟶

(ii) When the background acceptors prevail (i.e., $[A'_C] \gg [V''_{Ba}]$)

majority disorder	$n = 2[V_O^{\bullet\bullet}]$	$[A'_C] = 2[V_O^{\bullet\bullet}]$	$p = [A']$	$p = 2[V''_{Ba}]$
m_σ	$-1/6$	$-1/4, \quad +1/4$	0	$+1/6$
	———	Po_2 ———		⟶

These two possible sequences of majority disorder types are shown by the dotted lines in Figs. 8(a) and (b), respectively. (Since the cationic composition rather than a_{BaO} is fixed, the actual path is not necessarily a straight line in the configuration space of log Po_2 vs. log a_{BaO}.) It is likely that only the first two disorder regimes in any case must have been observed for the ''undoped'' specimen over the Po_2 range in Fig. 1 (i.e., $n = 2[V_O^{\bullet\bullet}]$ and then either $[V_O^{\bullet\bullet}] = [V''_{Ba}]$ or $[A'_C] = 2[V_O^{\bullet\bullet}]$ as Po_2 increases up to 1 atm). At this point, however, one cannot decide which of $[A'_C]$ and $[V''_{Ba}]$ is predominating, due to lack of precise enough data on chemical composition of the specimens employed.

The situation is somewhat different for a multivalent acceptor such as Mn. For Mn-doped $BaTiO_3$ where Mn is presently reconfirmed to act as an acceptor, the sequence of the m_σ values, Eq. (15), may be interpreted, in accord with Desu and Subbarao [7] and Osawa et al. [9], as follows. Even within the acceptor-dominating regime where $2[V_O^{\bullet\bullet}] = [\mathrm{Mn}'_{Ti}]$, the concentration of the acceptor $[\mathrm{Mn}'_{Ti}]$ may vary with Po_2 according to the ionization equilibrium

$$\mathrm{Mn}^x_{Ti} = \mathrm{Mn}'_{Ti} + h^\bullet; \quad K_A = \frac{[\mathrm{Mn}'_{Ti}]p}{[\mathrm{Mn}^x_{Ti}]} \tag{20}$$

where K_A denotes the ionization equilibrium constant. As the total amount of Mn is fixed or $[\mathrm{Mn}]_t = [\mathrm{Mn}^x_{Ti}] + [\mathrm{Mn}'_{Ti}] = 0.01$ in the present case,

$$[\mathrm{Mn}^x_{Ti}] = \frac{p[\mathrm{Mn}]_t}{p + K_A}; \quad [\mathrm{Mn}'_{Ti}] = \frac{K_A[\mathrm{Mn}]_t}{p + K_A} \tag{21}$$

At the lower Po_2, it is highly likely that $p \ll K_A$ and hence $[\mathrm{Mn}'_{Ti}] = [\mathrm{Mn}]_t$. Thus, due to Eqs. (4) and (16)–(19), one obtains

$$n = (2K_R)^{1/2}[\mathrm{Mn}]_t^{-1/2}Po_2^{-1/4};$$
$$p = K_i(2K_R)^{-1/2}[\mathrm{Mn}]_t^{1/2}Po_2^{1/4} \tag{22}$$

At the higher Po_2, $p \gg K_A$ and hence $[\mathrm{Mn}^x_{Ti}] = [\mathrm{Mn}]_t$. Thus, due to Eqs. (4), (16)–(20)

$$n = K_i^{1/3}(2K_R)^{1/3}K_A^{-1/3}[\mathrm{Mn}]_t^{-1/3}Po_2^{-1/6};$$
$$p = K_i^{2/3}(2K_R)^{-1/3}K_A^{1/3}[\mathrm{Mn}]_t^{1/3}Po_2^{1/6} \tag{23}$$

Within the regime of the majority disorder, $[\mathrm{Mn}'_{Ti}] = 2[V_O^{\bullet\bullet}]$, defect concentrations are therefore expected to vary against log Po_2 as shown in Fig. 9. The latter has been calculated at 1100°C from Eqs. (4), (16), (17), (19), and (21) with the numerical values $K_R/\mathrm{cm}^{-9}\,\mathrm{atm}^{1/2} = 1.44 \times 10^{50}$ [36], $K_i/\mathrm{cm}^{-6} = 1.56 \times 10^{34}$, $K_A/\mathrm{cm}^{-3} = 2.01 \times 10^{16}$ [Eq. (27) below], $[\mathrm{Mn}]_t/\mathrm{cm}^{-3} = 1.53 \times 10^{20}$, and $[A'_C]/\mathrm{cm}^{-3} = 3.06 \times 10^{18}$ (estimated from the purity of the starting powders). As clearly seen, the concentration of the major electronic carriers varies with increasing

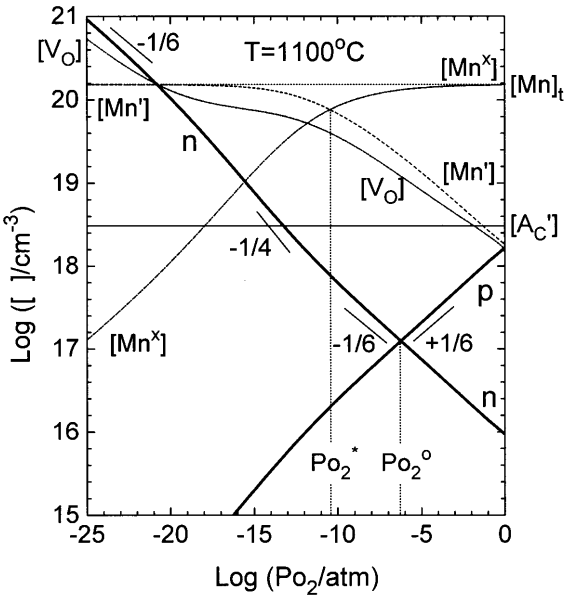

Fig. 9. Expected defect concentrations within the regime of $[\mathrm{Mn}'_{Ti}] = 2[V_O^{\bullet\bullet}]$, against oxygen partial pressure, for the Mn-doped $BaTiO_3$ at 1100°C. Note that the regime is further divided into two subregions where $[\mathrm{Mn}'_{Ti}] \gg [\mathrm{Mn}^x_{Ti};]$ and $[\mathrm{Mn}'_{Ti}] \ll [\mathrm{Mn}^x_{Ti};]$, respectively. For the calculation of defect concentrations, the following values were used: $K_R/\mathrm{cm}^{-9}\,\mathrm{atm}^{1/2} = 1.44 \times 10^{50}$ [36], $K_i/\mathrm{cm}^{-6} = 1.56 \times 10^{34}$, $K_A/\mathrm{cm}^{-3} = 2.01 \times 10^{16}$, $[\mathrm{Mn}]_t/\mathrm{cm}^{-3} = 1.53 \times 10^{20}$, and $[A'_C]/\mathrm{cm}^{-3} = 3.06 \times 10^{18}$ (based on the purity of the starting powders).

Po_2 as $n \propto Po_2^{-1/4}$, then $n \propto Po_2^{-1/6}$, and finally $p \propto Po_2^{+1/6}$ over the Po_2 range examined ($Po_2 \gtrsim 10^{-16}$ atm). This sequential variation has been reflected onto each of the conductivity isotherms in Fig. 2(a), yielding the sequence of m_σ values, Eq. (15). There would appear a region where $n \simeq 2[V_O^{\bullet\bullet}] \propto Po_2^{-1/6}$ in Fig. 2(a) if Po_2 went much lower than 10^{-16} atm. As $[Mn'_{Ti}]$ further decreases with increasing Po_2, the role of Mn'_{Ti} might likely be replaced by background acceptor-type impurities ($[A'_C] = 2[V_O^{\bullet\bullet}]$).

The validity of this defect structure of Mn-doped $BaTiO_3$, Fig. 9, is generally supported by the results of thermogravimetric study [8] and phase transition study [41]. As Po_2 decreases from 1 atm at 1000°C, mass of 1 *m/o* Mn-doped $BaTiO_3$ decreases (or $[V_O^{\bullet\bullet}]$ increases) monotonically and then becomes nearly arrested after passing approximately $\log(Po_2/\text{atm}) \approx -10$ [8]. The latter generally agrees with the boundary between the neighboring Po_2 regions where $m_\sigma = -1/6$ and $m_\sigma = -1/4$ in Fig. 2(a), that is $\log(Po_2^*/\text{atm}) = -10.2$ at 1000°C. (see Table 3) A monotonic decrease of the cubic-to-tetragonal phase-transition temperature with decreasing Po_2 is also arrested upon passing the equilibrium oxygen partial pressure, $\log(Po_2/\text{atm}) \approx -11$, for Mn-doped $BaTiO_3$ which has previously been equilibrated at 1000°C under controlled oxygen partial pressures and subsequently quenched [41]. This transition temperature of undoped $BaTiO_3$ has been known to decrease by $40 \sim 50$°C for every 10^{20} $V_O^{\bullet\bullet}$'s per cm^3 [42].

In Fig. 9, the oxygen partial pressures corresponding to the boundary between the two subregions, $[Mn]_t \simeq [Mn'_{Ti}] (\gg [Mn_{Ti}^x])$ and $[Mn]_t \simeq [Mn_{Ti}^x] (\gg [Mn'_{Ti}])$ and corresponding to $n = p$ are denoted as Po_2^* and Po_2°, respectively. These Po_2 values may be calculated from Eqs. (22) and (23):

$$Po_2^* = K_i^{-4}(2K_R)^2 K_A^4 [Mn]_t^{-2};$$
$$Po_2^\circ = K_i^{-1}(2K_R)^2 K_A^{-2}[Mn]_t^{-2} \quad (24)$$

One can immediately recognize that

$$K_A K_i^{-1/2} = (Po_2^*/Po_2^\circ)^{1/6} \quad (25)$$

The ionization equilibrium constant for Mn_{Ti}^x, K_A, can be evaluated provided that the values for Po_2^* and Po_2° and K_i are known. Taking the mobility ratio, b, to be of the order of 1 (c.f. $b \approx 3$ for hopping conduction), Po_2° may be taken as that corresponding to the conductivity minimum [Fig. 2(a), Table 1], and Po_2^* as that bordering the Po_2 exponent regions $2|m_\sigma| = 1/2$ and 1/3 [Fig. 3(b), Table 3]. By using these Po_2 values, $K_A K_i^{-1/2}$ is evaluated and plotted against the reciprocal temperature in Fig. 10. It is unclear why the datum for 1100°C falls far off the obvious trend in Fig. 10. Rejecting this particular datum, we may best estimate $K_A K_i^{-1/2}$ as

$$K_A K_i^{-1/2} = (1.224 \pm 0.002) \times \exp\left(\frac{-0.2274 \pm 0.0002\,\text{eV}}{kT}\right) \quad (26)$$

By substituting Eq. (13), one finally evaluates K_A as

$$K_A/\text{cm}^{-3} = 3.19 \times 10^{22} \times \exp\left(\frac{-1.69 \pm 0.02\,\text{eV}}{kT}\right) \quad (27)$$

It is pointed out that, whereas the value for the pre-exponential factor in Eq. (27) is dependent on the conduction mechanism assumed and, thus, subjected to ambiguity, the activation energy, $h_A = 1.69$ eV, is not. This has been determined experimentally on the basis of a single, plausible assumption $b \approx 1$. [If $b \approx 3$ instead, one would get $K_A/\text{cm}^{-3} = 5.05 \times 10^{22} \exp(-1.66\,\text{eV}/kT)$.] This energy corresponds to the enthalpy (h_A) of the ionization reaction, Eq. (18),

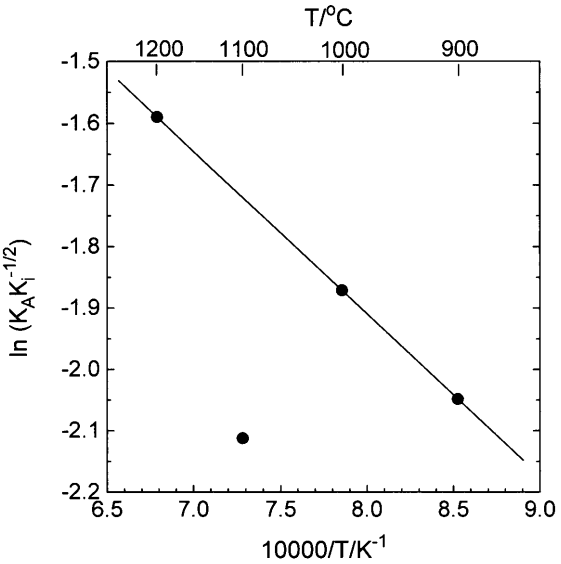

Fig. 10. $\ln K_A K_i^{-1/2}$ vs. reciprocal temperature. The solid line is the best-fitted with the datum at 1100°C rejected.

which has just been obtained experimentally for the first time of its kind for Mn-doped $BaTiO_3$.

Osawa et al. [9] have derived the same equilibrium constant as $K_A/\text{cm}^{-3} = 2.00 \times 10^{22} \exp(-1.2\ \text{eV}/kT)$ by fitting to their conductivity isotherms for Mn-doped $BaTiO_3$ (2 mole%) with the use of the literature value, $h_A = 1.2$ eV [43]. Their result appears to be in a reasonable agreement with Eq. (27). However, it is emphasized that they completely overlooked the presence of the region where $m_\sigma = -1/6$ upon the *n*-type branch of their conductivity isotherms.

V. Conclusions

It is unambiguously reconfirmed that Mn acts as an acceptor in Mn-doped $BaTiO_3$. The oxidation of Mn^{3+} to Mn^{4+} within the acceptor (Mn'_{Ti}) dominating region causes the major electronic carriers to vary as $n \propto Po_2^{-1/4}$ to $n \propto Po_2^{-1/6}$ to $p \propto Po_2^{+1/6}$ as Po_2 increases from 10^{-16} to 1 atm at elevated temperatures. The experimental values for Po_2 demarcating these three regions results in the equilibrium constant, K_A, for the reduction reaction $Mn^x_{Ti} = Mn'_{Ti} + h^{\cdot}$ as $K_A/\text{cm}^{-3} = 3.19 \times 10^{22} \exp(-1.69\ \text{eV}/kT)$.

Acknowledgment

The authors thank Dr. Nowotny at ANSTO, Australia for his careful reading of the manuscript and many valuable suggestions. This work was financially supported first by the Ministry of Trade, Industry and Energy via Industrial Generic Technique Development Program and later by Korea Science and Engineering Foundation via the Research Center for Thin Film Fabrication and Crystal Growing of Advanced Materials at Seoul National University.

References

1. M. Matsuoka, Y. Matsuo, H. Sasaki, and S. Hayagawa, *J. Am. Ceram. Soc*., **55**[2], 108 (1972).
2. H. Ueoka, *Ferroelectrics*, **7**, 352–53 (1974).
3. H.-J. Hagemann and H. Ihrig, *Phys. Rev. B*, **20**[9], 3871–3878 (1979).
4. H. Ihrig, *J. Am. Ceram. Soc*., **64**[10], 617–620 (1981).
5. T.R.N. Kutty and P. Murugarai, *Mater. Lett*., **3**[5–6], 195–198 (1985).
6. C.-J. Ting, C.-J. Peng, H.-Y. Lu, and S.-T. Wu, *J. Am. Ceram. Soc*., **73**[20], 329–334 (1990).
7. S.B. Desu and E.C. Subbarao, pp. 189–206 in *Advances in Ceramics*, Vol. 1, *Grain Boundary Phenomena in Electronic Ceramics*, ed. by L.M. Levinson, *Am. Ceram. Soc*., (Columbus, Ohio, 1981).
8. H.J. Hagemann and D. Hennings, *J. Am. Ceram. Soc*., **64**[10], 590–594 (1981).
9. S. Osawa, A. Furuzawa, and N. Fujikawa, *J. Am. Ceram. Soc*., **76**[5], 1191–1194 (1993).
10. H.-I. Yoo and J.-H. Hwang, *J. Phys. Chem. Solids*, **53**[7], 973–981 (1992).
11. S.A. Long and R.N. Blumenthal, *J. Am. Ceram. Soc*., **54**[10], 515–519 (1971).
12. A.M.J.H. Seuter, *Philips Res. Repts. Suppl*., **3**, 1–81 (1974).
13. J. Daniels and K.H. Härdtl, *Philips Res. Repts*., **31**, 489–504 (1976).
14. N.H. Chan and D.M. Smyth, *J. Electrochem. Soc*., **123**[10], 1584–1585 (1976).
15. N.G. Eror and D.M. Smyth, *J. Solid State Chem*., **24**, 235–244 (1978).
16. N.H. Chan, R.K. Sharma, and D.M. Smyth, *J. Am. Ceram. Soc*., **64**[9], 556–562 (1981).
17. J. Daniels, *Philips Res. Repts*., **31**, 505–515 (1976).
18. N.-H. Chan, R.K. Sharma, and D.M. Smyth, *J. Am. Ceram. Soc*., **65**[3], 167–170 (1982).
19. Y.H. Han, J.B. Appleby, and D.M. Smyth, *J. Am. Ceram. Soc*., **70**[2], 96–100 (1987).
20. H. Ikushima and S. Hayakawa, *J. Phys. Soc. Japan*, **19**, 1986 (1964).
21. H.-I. Yoo and C.-S. Kim, *Solid State Ionics*, **53–56**, 583–601 (1992); C.-S. Kim and H.-I. Yoo, *J. Electrochem. Soc*., **143**[9], 2863–2870 (1996).
22. J.H. Becker and H.P.R. Frederikse, *J. Appl. Phys*., **33**[1], 447–453 (1962).
23. J. Nowotny and M. Rekas, *Ceram. International*, **20**, 225–235 (1994).
24. E. Duverger, B. Jannot, M. Maglione, and M. Jannin, *Solid State Ionics*, **73**, 139–145 (1994).
25. M. DiDomenico, Jr. and S.H. Wemple, *Phys. Rev*., **166**[2], 565–576 (1968).
26. M. Cardona, *Phys. Rev*., **140**[2A], 651–655 (1965).
27. W.S. Baer, *J. Phys. Chem. Solid*., **28**, 677–687 (1967).
28. G.V. Lewis and C.R.A. Catlow, *J. Phys. Chem. Solids*, **47**[1], 89–97 (1986).
29. E.K. Chang, A. Mehta, and D.M. Smyth, pp. 35–45 in Proc. the Symposium on Electro-Ceramics, and Solid State Ionics, H.L. Tuller and D.M. Smyth, eds., (The Electrochem. Soc., Inc., NJ, 1988).
30. G.H. Jonker, *Philips Res. Repts*., **23**, 131–138 (1968).
31. C. Wagner, *Progr. Solid State Chem*., **7**, 1–37 (1972).
32. H. Ihrig, *J. Phys. C*, **9**, 3469–3474 (1976).
33. H. Ihrig and D. Hennings, *Phys. Rev. B*, **17**[12], 4593–4599 (1978).
34. J.P. Boyeaux and F.M. Michel-Calendini, *J. Phys. C*, **12**, 545–556 (1979).
35. E. Iguchi, N. Kuboto, T. Nakamori, N. Yamamoto, and K.J. Lee, *Phys. Rev. B*, **43**[10], 8646–8649 (1991).

36. J. Nowotny and M. Rekas, *Ceram. International*, **20**, 257–263 (1994).
37. H. Schmalzried, *Progr. Solid State Chem.*, **2**, 265–303 (1965).
38. N. Nowotny and M. Rekas, *Solid State Ionics*, **49**, 135–154 (1991).
39. G.V. Lewis and C.R.A. Catlow, *Radiat. Eff.*, **73**[1–4], 307–314 (1983).
40. J.F. Baumard and P. Abelard, *Solid State Ionics*, **12**, 47–51 (1984).
41. I. Burn, *J. Mat. Sci.*, **14**, 2453–58 (1979).
42. K.H. Härdtl and R. Wernicke, *Solid State Comm.*, **10**, 153–157 (1972).
43. R.M. Waser, *J. Am. Ceram. Soc.*, **72**[12], 2234–2240 (1989).